Research Article Vol. 14, No. 11 / 1 Nov 2023 / Biomedical Optics Express 5870
Biomedical Optics EXPRESS

Non-invasive assessment of hair regeneration in androgenetic alopecia mice *in vivo* using two-photon and second harmonic generation imaging

GAIYING HE,[1,†] MENGHUA LIU,[2,†] FENGLONG WANG,[2] SHUQING SUN,[3] YU CAO,[4] YANAN SUN,[1] SHUHUA MA,[1] AND YI WANG[1,*]

[1]*Experimental Research Center, China Academy of Chinese Medical Sciences, Beijing 100700, China*
[2]*School of Life Science, Beijing University of Chinese Medicine, Beijing 102488, China*
[3]*Institute of Biopharmaceutical and Healthcare Engineering, Shenzhen International Graduate School, Tsinghua University, Shenzhen 518055, China*
[4]*Institute of Geriatrics, Xiyuan Hospital, China Academy of Chinese Medical Sciences, Beijing 100091, China*
[†]These authors contributed equally to this work.
[*]*wangyi@merc.ac.cn*

Abstract: The identification of crucial targets for hair regrowth in androgenetic alopecia (AGA) involves determining important characteristics and different stages during the process of hair follicle regeneration. Traditional methods for assessing key features and different stages of hair follicle primarily involve taking skin tissue samples and determining them through various staining or other methods. However, non-invasive assessment methods have been long sought. Therefore, in this study, endogenous fluorescence signals from skin keratin and second harmonic signals from skin collagen fibers were utilized as probes, two-photon excited fluorescence (TPEF) and second harmonic generation (SHG) imaging techniques were employed to non-invasively assess hair shafts and collagen fibers in AGA mice *in vivo*. The TPEF imaging technique revealed that the alternation of new and old hair shafts and the different stages of the growth period in AGA mice were delayed. In addition, SHG imaging found testosterone reduced hair follicle area and miniaturized hair follicles. The non-invasive TPEF and SHG imaging techniques provided important methodologies for determining significant characteristics and different stages of the growth cycle in AGA mice, which will facilitate future non-invasive assessments on human scalps *in vivo* and reduce the use of animal testing.

1. Introduction

Alopecia is an affliction commonly encountered in clinical practice [1], with numerous types such as androgenetic alopecia (AGA), telogen effluvium, alopecia areata, and traction alopecia [2]. AGA is prevalent among both genders and affects about 85% of men and 40% of women [3,4]. AGA is a kind of alopecia that is mediated by dihydrotestosterone [5], is characterized by a progressive miniaturization of hair follicles, a shortened anagen phase, a prolonged telogen phase, and reduced hair density on the scalp. Alopecia can significantly lower patients' self-esteem and confidence, causing psychological distress [6]. The hair growth cycle consists of three distinct stages: the anagen phase, the catagen phase, and the telogen phase [7–10]. Each stage has unique structural features: the anagen phase is the stage of hair regeneration, the catagen phase is the stage of regression characterized by cell apoptosis, and the telogen phase is the relatively inactive phase of the follicle [11,12]. Since determining characteristics during hair follicle regeneration and identifying different stages of the hair growth cycle are vital for promoting hair regrowth and evaluating treatment efficacy, detection methods have become the focus of attention. However,

#503312 https://doi.org/10.1364/BOE.503312
Journal © 2023 Received 17 Aug 2023; revised 15 Sep 2023; accepted 20 Sep 2023; published 19 Oct 2023

Biomedical Optics EXPRESS

traditional methods to assess important characteristics and different stages of the hair growth cycle primarily involve sacrificing animals to obtain samples or performing scalp biopsies in humans and detecting them through various staining methods [13,14]. These methods result in animal waste and are not feasible for assessing hair regrowth in humans. Thus, developing non-invasive methods is urgently required for determining important characteristics and different stages of the hair growth cycle *in vivo*.

Few non-invasive methods exist for detecting and evaluating hair regrowth *in vivo*. While some studies assessed hair regrowth by measuring the length and growth rate of newly grown hair [15], others observed the morphology and pathological changes of plucked hair follicles to avoid the use of histological sections [16]. However, these methods do not provide crucial targets for determining the different stages of hair regeneration. Two-photon excited fluorescence (TPEF) and second harmonic generation (SHG) imaging techniques can visualize endogenous fluorophores and nonlinear optical imaging substances in skin tissue without requiring any fluorescent labels. The TPEF imaging principle involves the simultaneous excitation of ground-state electrons by two photons, transitioning from the excited state to the metastable state, and then returning to the ground state. The energy transition then emits fluorescence photons from the metastable state to the ground state. SHG imaging is a nonlinear optical process wherein two photons of the same frequency interact with a non-centrosymmetric substance, causing the molecules within the substance to undergo second-order nonlinear polarization due to intense laser light. This polarization results in the emission of coherent light of doubled frequency. TPEF and SHG imaging provide new techniques and evaluation methods for non-invasive visual research of skin tissue *in vivo*.

The skin is recognized to contain numerous endogenous fluorophores and second harmonic generation (SHG) signals generated by collagen fibers that are non-centrosymmetric in nature. Endogenous fluorophores that are present in the skin include keratin, melanin, nicotinamide adenine dinucleotide (NAD(P)H), flavin adenine dinucleotide (FAD) and other molecules. These fluorophores and collagen fibers possess specific excitation and emission wavelengths (Table 1), making them effective targets for non-invasive imaging techniques. Based on various studies [17–19], the hair keratin-associated protein, as the major structural component of hair fibers, is one potential target that can be utilized for identifying changes in hair shafts. In conclusion, TPEF and SHG imaging have been used to observe fluorophores and collagen fibers. However, the assessment of different growth phases and important characteristics for hair regrowth have not been reported based on hair shafts observed by keratin using TPEF imaging. In addition, there are fewer studies on predicting the size and duration of enlarged hair follicles using fluorescent signals from collagen by SHG imaging. In this study, we used TPEF and SHG imaging to observe important features and different stages in the process of hair follicle regeneration based on keratin and collagen.

Table 1. Excitation and emission wavelength of skin endogenous fluorophores and collagen.

Fluorophores	Location	λex (nm)	λem (nm)	Ref.
Keratin	Epidermis, dermis	760, 750	475	[20,21]
Melanin	Epidermis	730/780/830, 800	550, 620	[22,23]
NAD(P)H	Epidermis, dermis	750, 720	450, 460/60	[24,25]
FAD	Epidermis, dermis	850, 900	552/57, 525	[25,26]
Elastin	Dermis, subcutis	780/830, 800	475	[22,27]
Collagen	Dermis, subcutis	950, 830	1/2 laser wavelength	[22,28]

TPEF and SHG imaging techniques have gained widespread applications in various fields such as wound healing [29,30], transdermal processes [31,32], and identifying skin cancers [33,34]. Previous studies used transgenic mouse that marked the epithelial nuclei of skin by expressing a

Biomedical Optics EXPRESS

fusion protein of histone H2B with green fluorescent protein driven by the keratin 14 promoter (K14H2BGFP) [35,36], TPEF imaging detected hair follicle by marking the epithelial nuclei. To investigate neogenic hair follicle formation, epidermal stem cells (Epi-SCs) derived from neonatal C57BL/6 mice were labelled with tdTomato, and skin-derived precursors (SKPs) were isolated from neonatal C57BL/6/GFP mice, and reconstituting function of hair follicles from Epi-SCs and SKPs was tracked using TPEF imaging [37]. TRITC-conjugated dextran/FITC-conjugated dextran was injected into the tail vein to evaluate blood vessel leakage using TPEF imaging [38]. We found that TPEF imaging of hair regrowth relied largely on transgenic animal models and exogenous fluorescence labeling, which make such methods complex and costly, and impractical for widespread use. To overcome these limitations, a novel approach is proposed in this study, whereby the endogenous fluorescence signals of keratin and the unique optical characteristics of collagen fibers were harnessed as natural probes. This enabled direct and non-invasive investigations of changes occurring in the hair shafts and hair follicles during the complete growth cycle in AGA mice using TPEF and SHG imaging techniques. Additionally, traditional methods were employed for validation purposes. The results of this study indicate that by utilizing endogenous fluorescence signals and collagen fibers as natural probes, an effective approach for the non-invasive evaluation of important characteristics of hair regeneration and different stages

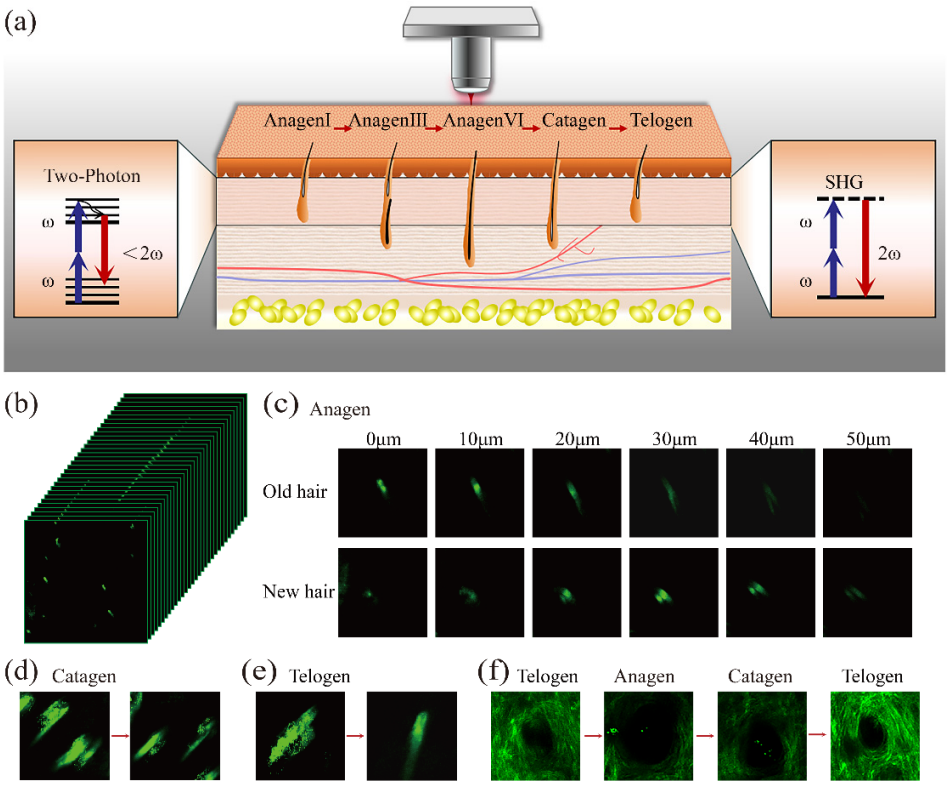

Fig. 1. The pathological changes during the different stages of the growth cycle using TPEF and SHG imaging. (a) Schematic diagram of TPEF and SHG imaging on hair regeneration. (b) Different depths imaging of keratin fluorescence signals from hair shafts using TPEF imaging. (c) In anagen, fluorescence signals of hair shafts at different depths reveal changes of new and old hair shafts. (d) Changes of the hair shaft during the anagen-catagen phase using TPEF imaging. (e) Changes of the hair shaft during the catagen-telogen phase using TPEF imaging. (f) Change of hair follicle size during the growth cycle.

Biomedical Optics EXPRESS

of the growth cycle is achieved, the experimental process are illustrated in Fig. 1. Consequently, this research has the potential to significantly impact the field of hair biology, reduce the reliance on experimental animals, and pave the way for future non-invasive assessments of human scalps.

2. Materials and methods

2.1. Animal preparation

All animal experimental procedures were approved by the Institutional Animal Care and Use Committee of the Experimental Research Center, China Academy of Chinese Medicine Science (protocol code ERCCACMS11-2210-03). A total of 66 male C57BL/6 mice, with a weight range of 20 ± 2 g, were procured from Beijing Vital River Laboratory Animal Technology (Beijing, China). These mice were then allocated randomly into two groups, namely the control (CON) group and the testosterone (TES) group (Standard, Shanghai, China). Devoid of hair, the back of each mouse was shaved using depilatory cream. A day after depilation, the TES group received topical application of testosterone at a concentration of 1 mg/mL, employing a dosage of 0.15 mL per application. In contrast, the CON group received solvent instead. For a period of 26 days, this treatment was administered once per day.

2.2. TPEF imaging

For non-invasive imaging, a two-photon excited fluorescence microscopy system (FV1000, Olympus, Japan) was employed. The TPEF Imaging system was equipped with a water-immersion objective lens (PLAN 25X OB. W IMM, NA 1.05, Olympus) and a Ti:sapphire laser oscillator (wavelength: 690-1040 nm; repetition rate: 80 MHz, pulse width: 100 fs; MaiTai HP DS-OL, Spectra-Physics, Inc. CA). Before imaging, the mice were anesthetized using isoflurane and were securely fixed onto the TPEF microscopy object stage. To minimize the effects of breathing movements, the skin was carefully stabilized using a holder throughout the imaging process. TPEF imaging technology was utilized to detect the signal emanating from the hair shafts, employing an excitation wavelength of 750 nm [21]. The emitted fluorescence signal was captured, covering the wavelength range of 420 to 460 nm, from the upper surface of the dermis. Imaging sessions were conducted once every two days, with data acquisition performed at regular intervals from day 2 to day 26. Each image set consisted of TPEF image stacks with a depth of 60 µm and 30 sections, acquired at a resolution of 1024×1024 pixels, a step size of 2 µm, and a scanning speed of 4 µs/pixel. Overall time of each image set was 120 s, the lateral and axial resolution was 0.9 µm x 1.8 µm, the images size was 510 µm x510 µm.

2.3. SHG imaging

Collagen fibers, which generated second harmonic signals, were detected by two-photon microscopy, utilizing an excitation wavelength of 950 nm and an emission filter of 475/20 nm [28]. This particular setup permitted the visualization of dynamic collagen fibers surrounding the hair follicles. The imaging process achieved a scanning depth of 45 µm and 22 sections, with the images captured at a resolution of 1024×1024 pixels, a step size of 2 µm, and a scanning speed of 4 µs/pixel, overall time of each image set was 90 s, lateral and axial resolution was 1 µm x 2 µm, the images size was 510 µm x510 µm. The utilization of these optimized imaging parameters enabled the acquisition of high-quality images, facilitating accurate assessment and quantification.

2.4. Hematoxylin and eosin staining

From day 2 to day 26, skin tissues were collected once every two days from the CON and TES groups. The skin tissues were then fixed, paraffin-embedded, and sectioned into 6 µm-thick slices using a microtome (Thermo Fisher Scientific, Waltham, MA, USA). Hematoxylin and Eosin

Biomedical Optics EXPRESS

(H&E) staining was used to stain the skin slices, which were subsequently observed employing an inverted microscope (Olympus BX51, Tokyo, Japan).

2.5. Liquid crystal polarized imaging

Skin tissues collected from both the CON and TES groups were fixed for 24 hours in 4% paraformaldehyde, embedded, and sectioned into 6 μm-thick slices. Post-dewaxing, the collagen fibers were observed and analyzed via liquid crystal polarizing imaging (CRi Abrio, America).

2.6. Statistical analyses

For data analysis, a t-test was conducted using SPSS v26.0 (IBM, Armonk, NY, USA). All data were then expressed as mean ± standard deviation (SD). Graphs were created employing Prism v8.0 (GraphPad, La Jolla, CA, USA). A significance level of $P<0.05$ was utilized to establish statistical significance.

3. Results

3.1. Investigation of hair regeneration and changes occurring at different stages during the growth cycle in AGA mice

AGA mice provide an important animal model for studying hair regeneration [39–41]. However, research on the pathological changes occurring throughout the entire growth cycle of AGA mice is limited. To observe the changes throughout this entire growth cycle, we selected the telogen phase at 7 8 weeks for the experiment (Fig. 2(a)). Considering that depilation-induced anagen is fully synchronized [14], hair was depilated before the experiment. Hair growth on shaved C57BL/6 mice was monitored every two days from day 2 to 26, as shown in Fig. 2(b).

To non-invasively detect changes during different stages and to capture vital features of hair follicles using TPEF and SHG imaging, traditional methods were initially employed to evaluate pertinent features during different stages. Sagittal plane sections of skin tissue, stained with hematoxylin-eosin (HE), served as a crucial criterion for hair regeneration assessment. Figure 2(c) shows the HE staining of sagittal plane sections at different times, while Fig. 2(d) represent the statistical analysis of follicle length. In the CON group, follicle length increased on day 6, with a peak observed on day 14 and day 16. Similarly, in the TES group, the increase was observed on day 8 with a peak seen on day 16 and day 18. Nevertheless, the maximum values of follicle length, and hair bulb diameter were lower than the corresponding values in the CON group. On day 24, both groups returned to the telogen phase. The results of the experiment signify that the presence of testosterone reduces follicle length, thereby leading to follicle miniaturization.

The current study utilized HE staining to identify the crucial growth stages of hair follicles, and the results were presented in Fig. 2(e). In the TES group, the hair bulbs were located at the border between the dermis and subcutis on day 8, corresponding to the anagen III phase, whereas new hair growth emerged on day 14, indicating progression to the anagen VI phase. However, anagen III and VI of AGA mice were found to be delayed compared to the CON group. Furthermore, the TES group entered into catagen III and catagen V phases on day 20 and day 22, respectively, sooner than the CON group. The hair follicles ultimately entered into the telogen phase on day 24. The growth stages were summarized based on the pathological changes at different times, and the findings are presented in Fig. 2(f). These results illustrate that testosterone not only delays the entry into the anagen phase of hair follicles but also shortens the anagen phase. Moreover, this study provides a foundation for the potential non-invasive identification of different stages during the follicle growth cycle.

Biomedical Optics EXPRESS

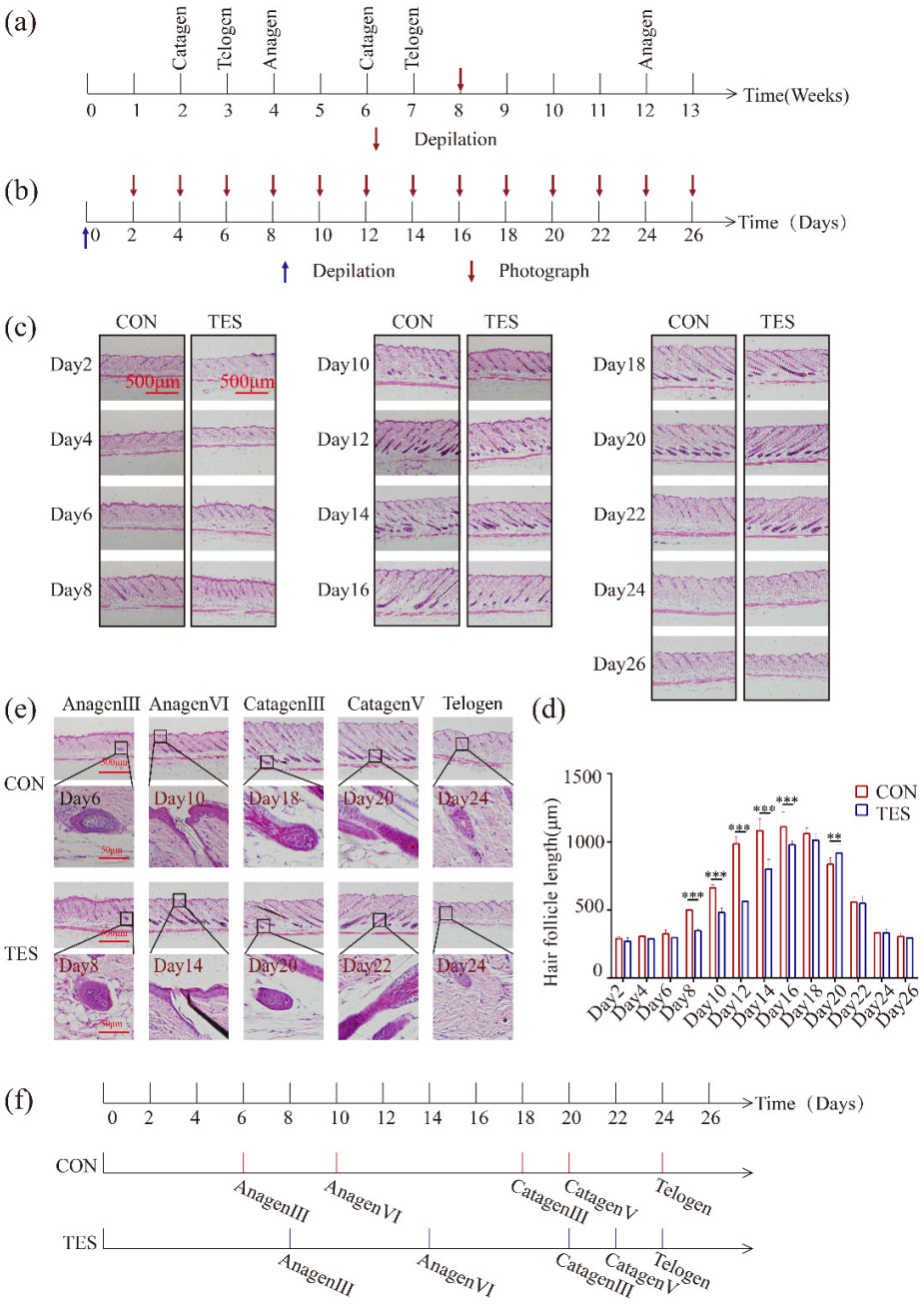

Fig. 2. Pathological changes at different stages of the hair growth cycle in AGA mice. (a) Schematic diagram of the hair growth cycle in mice. (b) Schematic diagram of the experimental treatment in mice. (c) HE staining images of skin sagittal plane at different stages of the growth cycle. (d) Statistical graph of hair follicle length at different stages of the growth cycle. (e) Typical images at different stages of the growth cycle. (f) Summary diagram of different growth stages during the growth cycle. Compared with the CON group, $*P < 0.05$, $**P < 0.01$, $***P < 0.001$.

Biomedical Optics EXPRESS

3.2. Changes of hair shafts during the growth cycle in AGA mice

To investigate changes in hair shafts during the growth cycle of AGA mice, we utilized TPEF imaging to examine the shafts from the upper surface of the dermis up to a depth of 60 µm. Additionally, we collected a hair shaft that had completed a full growth cycle and analyzed it using TPEF imaging techniques at the root, middle, and tip (Fig. 3(a)). The findings indicated that the root of the hair shaft had a uniform fluorescence signal and diameter without melanin, signifying it as a club hair. Conversely, the tip of the hair shaft gradually thickened from the top, whereas the middle portion exhibited a non-uniform fluorescence signal due to pigmented hair. These results have significant implications for the in vivo detection of essential hair shaft regeneration characteristics across different stages of the growth cycle.

Hair shafts were examined at different time intervals using TPEF imaging, and corresponding images and hair shaft diameters were shown in Fig. 3(b) and (c), respectively. In the control group, hair shafts demonstrated consistent fluorescence intensity until day 8, followed by a significant increase in thickness on day 12. It was observed that hair shafts differentiated on day 14, exhibiting a pattern of one coarse hair shaft surrounded by 2/3 fine hair shafts, which persisted until day 18. After day 20, hair shafts gradually thinned down. On the other hand, in the TES group, uniform fluorescence intensity was observed before day 12, differentiation was observed on day 16 and uniform fluorescence was observed on day 24. The diameters of coarse and fine hair shafts were compared between the two groups, and it was found that the hair shaft diameters were lower in the TES group when compared to the CON group. Furthermore, the changes in hair shafts observed using traditional HE staining were consistent with the findings obtained with TPEF imaging methodology (Fig. 3(d)). In conclusion, non-invasive TPEF imaging can be used to evaluate the effect of testosterone, and it is shown that testosterone leads to a decrease in the diameter of newly regenerated hair shafts.

3.3. Changes of new and old hair shafts at different stages of growth cycle in mice

3.3.1. Changes of new and old hair shafts at different stages of growth cycle in normal mice

We conducted TPEF imaging to investigate changes in newly regenerated and pre-existing hair shafts during various stages of the growth cycle in normal mice. By analyzing characteristics such as fluorescence signal depth, thickness, and melanin presence in hair shafts within a depth of 60µm, we identified the stages of the growth cycle and observed the alternating patterns between new and pre-existing hair shafts.

On day 4, hair shafts displayed robust fluorescence signal from 0µm to 40µm in the dermis, but the signal weakened at 50µm depth as a result of skin scattering, as illustrated in Fig. 4(a). Analysis of HE-stained samples confirmed that these hair shafts were old hair shafts (Fig. 2(c)). On day 6, two distinct categories of hair shafts were observed, with varying fluorescence signal intensities at different depths. One category of hair shafts demonstrated the same fluorescence signal as old hair shafts, whereas the other category had no fluorescent signal between 0µm and 40µm, but revealed a faint signal at 50µm depth, as demonstrated in Fig. 4(b). Based on staining results displayed in Fig. 2(c), these hair shafts were recognized as newly regenerated hair shafts. Literature findings suggest that hair shafts reach the location of the sebaceous gland during anagen III [14], hence, the hair on day 6 was identified to be in anagen III stage. By day 8, as old hair shafts progressed upwards, the signal emitted by old hair shafts weakened significantly at around 30µm depth. In contrast, the fluorescence signal of newly regenerated hair shafts gradually increased from 20µm depth, which corresponds to the position of the canal. This pattern signified that the hair follicles were entering the anagen V phase. The results are displayed in Fig. 4(c). On day 10, hair shafts emitted a fluorescence signal from 0 µm, and HE staining confirmed them to be new hair shafts (Fig. 2(c)). At this point, hair shafts were emerging onto the skin surface, indicating that the stage on day 10 was probably the anagen VI growth

Biomedical Optics EXPRESS

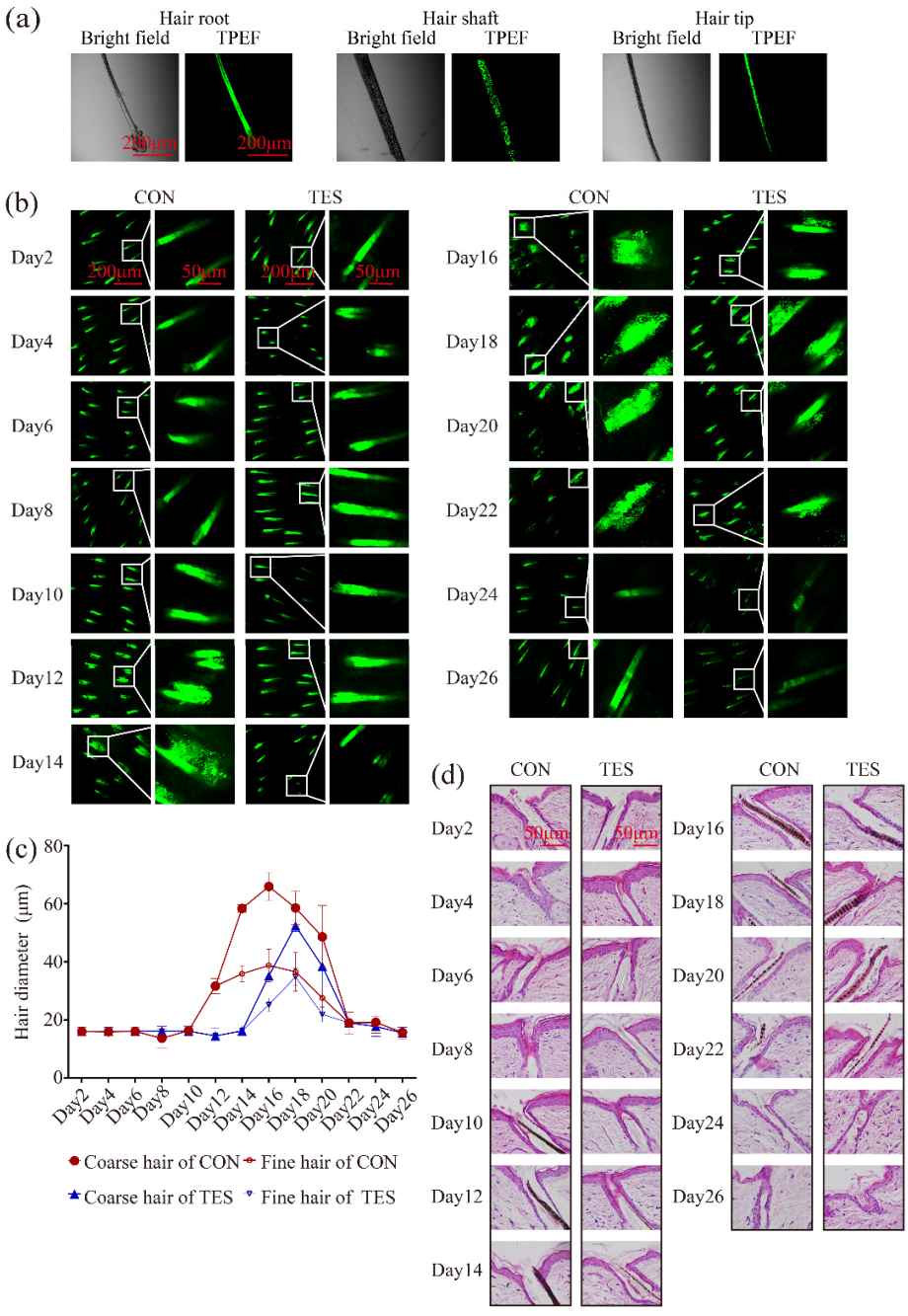

Fig. 3. Changes of the hair shafts at different stages of the growth cycle in AGA mice. (a) Images of the hair shaft at different positions using TPEF imaging after plucking. (b) Changes of the hair shafts at different stages of the growth cycle using TPEF imaging. (c) Diameter of the hair shafts at different stages of the growth cycle using TPEF imaging. (d) Changes of the hair shafts at different stages of the growth cycle using HE staining.

Biomedical Optics EXPRESS

phase. The results are shown in Fig. 4(d). However, from day 16 to 18, hair shafts became thinner, suggesting that hair follicles had entered the catagen phase (Fig. 4(e)). Finally, on day 24, hair shafts in both groups lacked melanin, signifying the end of hair shaft growth and the beginning of the telogen phase (Fig. 4(f)).

The outcomes of this study confirm that non-invasive TPEF imaging is a valuable technique for identifying the beginning of the anagen phase, determining the duration of the anagen phase, and estimating the timing of the catagen and telogen phases.

3.3.2. Changes of new and old hair shafts at different stages of the growth cycle in AGA mice

To better examine the changes in newly regenerated hair shafts and the rotation of new and old hair shafts in the TES group, we compared this group's results with those of the CON group, as illustrated in Fig. 5(a). In the TES group, HE staining confirmed that hair shafts were old on day 6, but by day 8, a few newly regenerated hair shafts had emerged, indicating the anagen III phase. It was observed on day 12 that new hair shafts had reached the canal, indicating that the TES group was in its anagen V stage. By day 14, some new hair shafts had reached the surface of the skin, indicating that the TES group was in its anagen VI phase. These findings show that the emergence of different stages in the TES group was delayed compared to the CON group. From days 18 to 20, hair shafts in the TES group became thinner, indicating that the hair follicles were entering the catagen phase (Fig. 5(b)). On day 24, hair follicles in both groups entered the telogen phase simultaneously (Fig. 5(c)). The growth stages were summarized based on TPEF imaging at different times, and the results are shown in Fig. 5(d). Overall, these results suggest that testosterone influences the rotation of new and old hair shafts, and it also leads to shortening of hair shaft growth.

3.4. Change of hair follicle size during the growth cycle in AGA mice

Hair follicles exhibit distinct shapes and sizes during different stages of the growth cycle. The structure of hair follicle comprises the outer root sheath, inner root sheath, and hair shaft, which are enclosed by connective tissue sheath containing collagen fibers and dermal collagen fibers. To examine variations in the fluorescence signal of collagen fibers encompassing the hair follicles, this study utilized SHG imaging technology. Given the absence of non-centrosymmetric symmetry structures in the hair follicle region, there is no observable fluorescence signal within the hair follicle itself. Therefore, changes in hair follicle dimensions can be assessed on the basis of the observed fluorescence signal in the surrounding collagen fibers.

Based on the findings presented in Fig. 6(a) and (b), the hair follicles demonstrated small areas from day 2 to day 4. Subsequently, on day 6, some hair follicles displayed increased area before the hair shafts grew out of the skin. From day 10 to day 18, the hair follicles in the CON group significantly augmented in size. In contrast, in the TES group, the hair follicles exhibited small areas before day 6, with individual hair follicles enlarging on day 8. Although the hair follicles in the TES group increased in size from day 12 to 16, their average follicle area was relatively smaller than that of the CON group. From day 22 to day 26, a reduction in the follicle areas was observed in both groups. Furthermore, changes in follicle size were assessed by liquid crystal polarizing imaging on skin tissue samples taken at various time points, and the results aligned with those obtained through SHG imaging technology (Fig. 6(c) and (d)). The study outcomes suggest that testosterone administration delays the emergence of enlarged hair follicles and decreases their size, as observed by SHG imaging technology.

Biomedical Optics EXPRESS

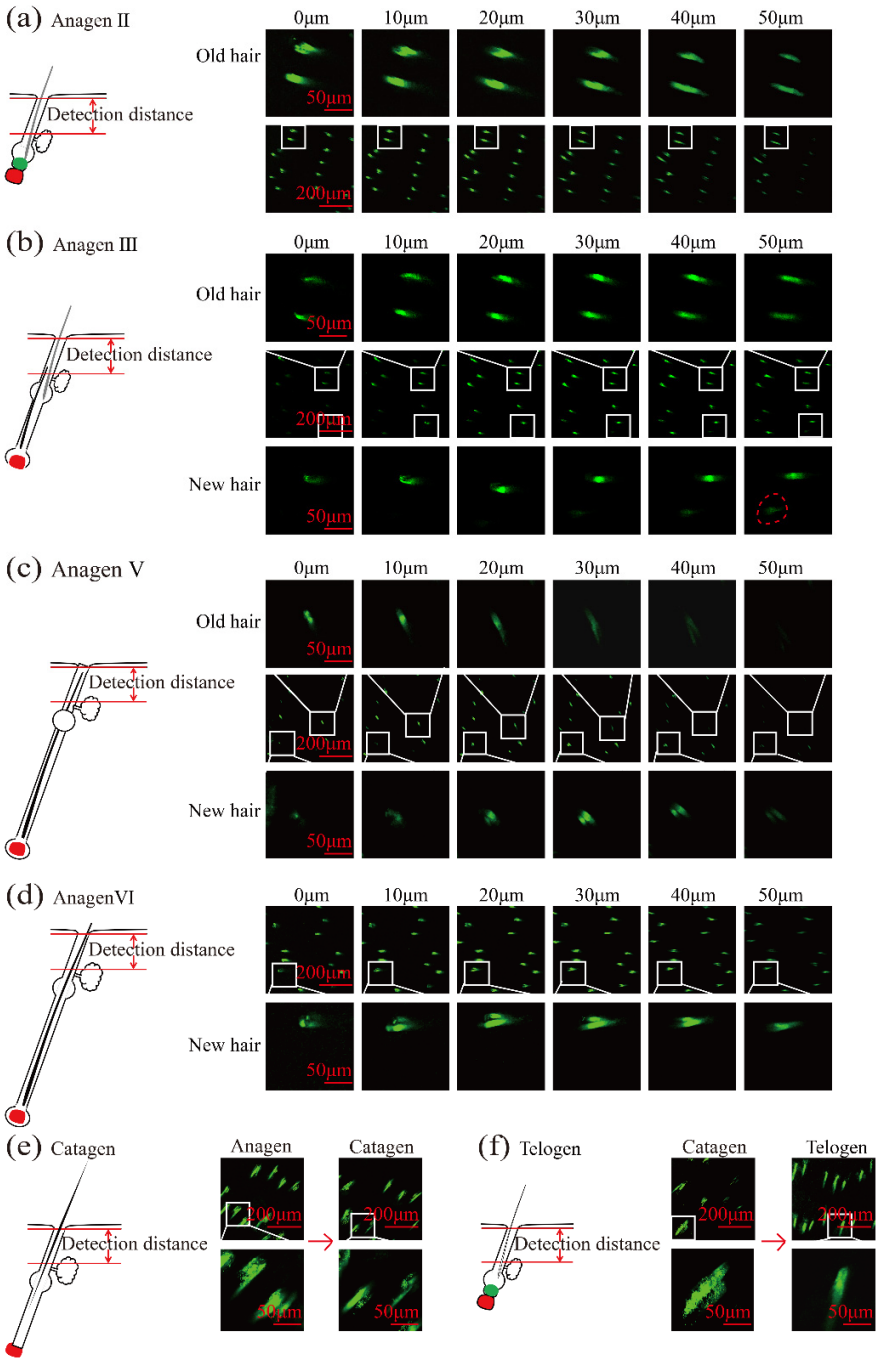

Fig. 4. Changes of new and old hair shafts at different stages during the growth cycle in normal mice. (a) Hair pattern and changes of hair shafts at different depths during anagen II on day 4. (b) Hair pattern and changes of hair shafts at different depths during anagen III on day 6. (c) Hair pattern and changes of hair shafts at different depths during anagen V on day 8. (d) Hair pattern and changes of hair shafts at different depths during anagen VI on day 10. (e) Hair patterns and changes of hair shafts from anagen to catagen on day 16 and day 18. (f) Hair patterns and changes of hair shafts from catagen to telogen on day 22 and day 24.

Biomedical Optics EXPRESS

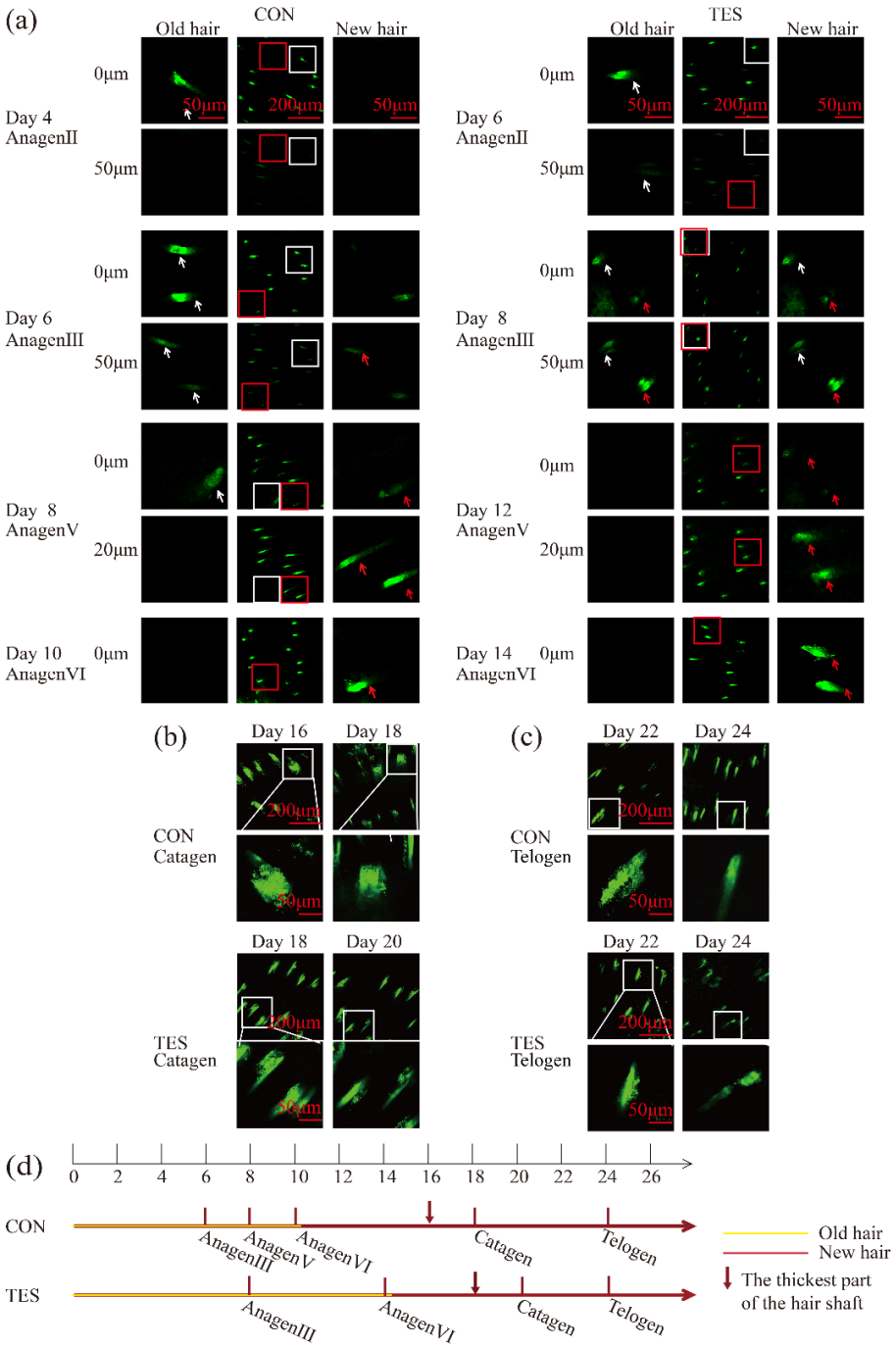

Fig. 5. Changes of new and old hair shafts at different stages of the growth cycle in AGA mice. (a) Changes of new and old hair shafts during the anagen phase. no new hair shaft in the control group on day 4 and in the TES group on day 6, no old hair shaft in the control group on day 10 and in the TES group on day 12 and 14. (b) Changes of hair shaft during the catagen phase. (c) Changes of hair shaft during the telogen phase. (d) Summary diagram of different growth stages during the growth cycle. White boxes and arrows represent old hair shafts, while red boxes and arrows represent new hair shafts.

Biomedical Optics EXPRESS

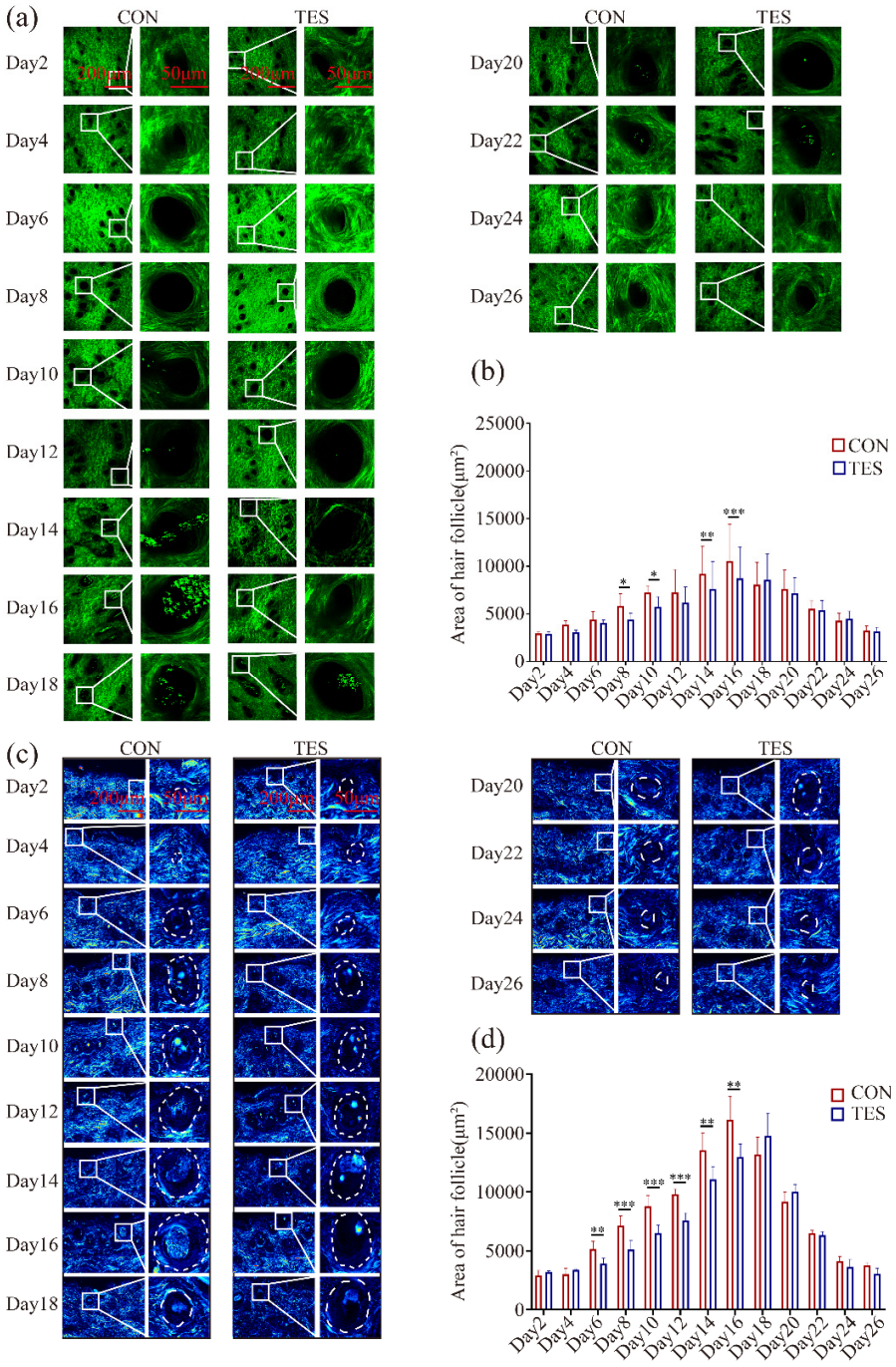

Fig. 6. Changes of hair follicle size during the growth cycle in AGA mice. (a) Change of hair follicle size detected by SHG imaging. (b) Statistical graph of hair follicle size detected by SHG imaging. (c) Changes of hair follicle size detected by liquid crystal polarizing imaging. (d) Statistical graph of hair follicle size detected by liquid crystal polarizing imaging. Compared with the CON group, $*P < 0.05$, $**P < 0.01$, $***P < 0.001$.

Biomedical Optics EXPRESS

4. Discussion and conclusions

AGA is characterized by progressive miniaturization of hair follicles and shortening of anagen phase. AGA is mainly caused by androgen hormones, an elevated local concentration of dihydrotestosterone (DHT). Other factors, such as UV light, pollutants and irritants have also been found to promote AGA [42]. Under androgens and irritants, the dermal papilla of hair follicles secrets many cytokines that can induce the anagen phase premature termination and stimulate catagen entry [43]. Study found Bmp2/4 and Fgf18 from dermal papilla inhibit stem cell activation [44]. However, the cyclic growth of hair follicles is driven by hair follicle stem cells. Multiple signalling pathways are involved in the pathogenesis of AGA, such as the Wnt/β-catenin pathway [45,46], Shh/Gli pathways [47], Notch pathway, BMP (bone morphogenetic proteins) pathway and apoptotic pathway [48], and so on.

The hair shaft comprises the cuticle, cortex, and medulla [49]. In anagen III, the cortex and medulla gradually develop in the newly formed hair shaft, and melanin begins to appear. During anagen IV and V, a substantial amount of melanin is present in the hair shafts [13,14]. In the middle to late stages of anagen, the hair canal contains at least two hair shafts: one being the club hair from the previous telogen phase, and the other being the newly formed hair shaft [14]. During the telogen phase, the hair shafts within the skin are identified as club hairs, which are colorless structures consisting of keratinized corneocytes at the proximal end of the hair follicle. The hair shaft appearance location within the skin has been recognized in earlier studies as a relevant indicator of anagen III, V, and VI. Specifically, anagen III is distinguished by the hair shaft's appearance at the opening of the sebaceous gland, anagen V by the tip of the hair shaft entering the hair canal, and anagen VI by the hair shaft reaching the surface of the skin [14].

Traditional methods typically involve staining pathology samples and examining the new hair shafts to differentiate the distinct stages of anagen. However, in this study, TPEF imaging demonstrated robust and coherent fluorescence signals of hair shafts at varying skin depths, suggesting that the hair shafts within the skin were old hairs/club hairs. The hair shafts gradually emerged at the opening of the sebaceous gland, hair canal, and surface of the skin, corresponding to anagen phases III, V, and VI, respectively. Notably, the anagen phases observed in the TES group were significantly postponed compared to the CON group. Furthermore, TPEF imaging indicated that the diameters of new hair shafts were relatively smaller in the TES group than those in the CON group. By evaluating the hair shaft's thickness and melanin presence in the hair shaft, the catagen and telogen stages could be recognized, respectively. These study findings suggest that TPEF imaging technology provides a vital non-invasive approach to evaluating hair shaft regeneration and distinguishing the diverse stages of the hair growth cycle.

From a cross-sectional perspective, the hair follicle can be divided into the outer root sheath, companion layer, inner root sheath, and hair shaft. The entire follicular epithelium is encompassed by a connective tissue sheath derived from the mesoderm, which directly contacts the dermal matrix predominantly composed of collagen I [50]. Earlier studies have shown that the hair follicle's size and structure undergo changes across different stages of the growth cycle [51,52]. These changes are fundamental to hair regeneration, but they are generally observed through pathological tissue samples. In this study, we utilized a non-invasive SHG imaging technique to identify changes in the fluorescence signal of collagen fibers surrounding the hair follicles and determine variations in hair follicle size. Our results indicated that in the TES group, the emergence of large hair follicles was postponed in comparison to the CON group. Additionally, the duration of the large hair follicle area was shorter in the TES group than in the CON group during the middle and late anagen and catagen stages. Therefore, through use of SHG imaging to observe the changes in follicle size throughout the growth cycle, we can gain insights into two crucial aspects. Firstly, it enables the assessment of whether hair follicles are entering the growth phase before the emergence of hair shafts from the skin, providing an invaluable approach for

Biomedical Optics EXPRESS

early detection of hair regeneration. Secondly, SHG imaging provides a non-invasive method of determining the effectiveness of hair growth treatments based on follicle size and duration.

TPEF and SHG imaging have been increasingly used in the study of skin and its appendages. Compared with single-photon imaging, TPEF imaging uses two photons with longer wavelengths (infrared spectrometry), which make stronger penetration owing to reduced light scattering from tissues, decrease phototoxicity and photobleaching [36,53]. In this study, TPEF imaging demonstrated different fluorescence characteristics of new hair, old hair/club hair, and identified the different stages of growth cycle based on the emergence location, diameter, and melanin of hair shafts, which was crucial for the pharmacodynamic assessment of hair regrowth. In addition, SHG imaging suggested the change of hair follicle dimensions could be assessed based on fluorescence signal from the surrounding collagen fibers. The size and duration of augmented hair follicles throughout the entire growth cycle were important features for early determination of hair regrowth, the thickness and length of hair. In conclusion, TPEF and SHG imaging are crucial for determining characteristics and growth cycle stages during the process of hair follicle regeneration. While TPEF and SHG imaging techniques have been increasingly utilized in skin disease research, their restricted penetration depth remains a significant challenge. Despite this limitation, it is hoped that TPEF and SHG imaging techniques can be further developed to overcome these issues and be widely employed in future research.

Hair follicle cells, such as hair follicle stem cells, outer root sheath cells, and inner root sheath cells, play an important role in each growth phase and hair regeneration. Previous study found that hair regeneration depended on the activation of hair follicle stem cells [54]. Outer root sheath cells maintained the hair follicle structure and supported the bulge area [55]. In the loose anagen hair syndrome, irregular keratinization of the cuticle cells of the inner root sheath and a swollen appearance of Huxley cells were found [56]. In our study, we used wild-type mice, TPEF imaging did not observe hair follicle cells. In the future, we hope to use transgenic animals marking the epithelial nuclei of skin, and study hair follicle cells and mechanisms of hair regeneration using TPEF and SHG imaging.

In this study, we employed non-invasive TPEF and SHG imaging techniques to explore the pathological changes during the different stages of the growth cycle in AGA mice by utilizing endogenous fluorescence signals and collagen fibers as natural probes. Specifically, TPEF imaging technology was utilized to monitor the changes in the hair shafts at various depths during the anagen phase. Our study revealed that the emergence of new hair shafts in AGA mice was postponed in comparison to the CON mice, and the duration of the growth period was relatively shorter in the AGA group. Furthermore, SHG imaging enabled us to observe the impact of testosterone on hair follicles, leading to the identification of delayed hair follicle enlargement and hair follicle miniaturization. These critical features, coupled with the recognition of diverse growth stages, not only offer a valuable non-invasive approach for assessing hair regeneration in AGA mice but also provide technical support for evaluating drug-induced hair regeneration in humans in vivo.

Funding. Youth Fund of the National Natural Science Foundation of China (82204902); The Fundamental Research Funds for the Central Public Welfare Research Institutes (JJPY2022001, RXRC2022004, XTCX2021002).

Disclosures. The authors declare no conflicts of interest.

Data availability. The data presented in this study are available in this article.

References

1. T. Mubki, L. Rudnicka, M. Olszewska, and J. Shapiro, "Evaluation and diagnosis of the hair loss patient: part I. History and clinical examination," J. Am. Acad. Dermatol. **71**(3), 415 (2014).
2. A. Villani, G. Fabbrocini, J. Ocampo-Candiani, A. Ruggiero, and S. S. Ocampo-Garza, "Review of oral minoxidil as treatment of hair disorders: in search of the perfect dose," J. Eur. Acad. Dermatol. **35**(7), 1485–1492 (2021).
3. S. Chen, X. Xie, G. Zhang, and Y. Zhang, "Comorbidities in androgenetic alopecia: a comprehensive review," Dermatol. Ther. **12**(10), 2233–2247 (2022).

Biomedical Optics EXPRESS

4. A. K. Gupta, R. R. Mays, M. S. Dotzert, S. G. Versteeg, N. H. Shear, and V. Piguet, "Efficacy of non-surgical treatments for androgenetic alopecia: a systematic review and network meta-analysis," J. Eur. Acad. Dermatol. Venereol. **32**(12), 2112–2125 (2018).
5. A. Adil and M. Godwin, "The effectiveness of treatments for androgenetic alopecia: A systematic review and meta-analysis," J. Am. Acad. Dermatol. **77**(1), 136–141.e5 (2017).
6. K. York, N. Meah, B. Bhoyrul, and R. Sinclair, "A review of the treatment of male pattern hair loss," Expert Opin. Pharmacother. **21**(5), 603–612 (2020).
7. J. Legrand, R. Villani, E. Roy, and K. Khosrotehrani, "STAT5 activation in the dermal papilla is important for hair follicle growth phase induction, hair follicle regeneration and wound healing," J. Invest. Dermatol. **136**(9), 1781–1791 (2016).
8. B. Y. Choi, "Hair-growth potential of ginseng and its major metabolites: a review on its molecular mechanisms," Int. J. Mol. Sci. **19**(9), 2703 (2018).
9. W. J. Suen, S. T. Li, and L. T. Yang, "Hes1 regulates anagen initiation and hair follicle regeneration through modulation of hedgehog signaling," Stem Cells **38**(2), 301–314 (2020).
10. S. M. Kim, J. I. Kang, H. S. Yoon, Y. K. Choi, J. S. Go, S. K. Oh, M. Ahn, J. Kim, Y. S. Koh, J. W. Hyun, E. S. Yoo, and H. K. Kang, "HNG, a humanin analogue, promotes hair growth by inhibiting anagen-to-catagen transition," Int. J. Mol. Sci. **21**(12), 4553 (2020).
11. M. R. Schneider, R. Schmidt-Ullrich, and R. Paus, "The hair follicle as a dynamic miniorgan," Curr. Biol. **19**(3), R132–R142 (2009).
12. X. Lin, L. Zhu, and J. He, "Morphogenesis, growth cycle and molecular regulation of hair follicles," Front. Cell. Dev. Biol. **10**, 899095 (2022).
13. J. W. Oh, J. Kloepper, E. A. Langan, Y. Kim, J. Yeo, M. J. Kim, T. C. Hsi, C. Rose, G. S. Yoon, S. J. Lee, J. Seykora, J. C. Kim, Y. K. Sung, M. Kim, R. Paus, and M. V. Plikus, "A guide to studying human hair follicle cycling in vivo," J. Invest. Dermatol. **136**(1), 34–44 (2016).
14. S. Muller-Rover, B. Handjiski, C. van der Veen, S. Eichmuller, K. Foitzik, I. A. McKay, K. S. Stenn, and R. Paus, "A comprehensive guide for the accurate classification of murine hair follicles in distinct hair cycle stages," J. Invest. Dermatol. **117**(1), 3–15 (2001).
15. M. D. Schuldenfrei and J. B. Pieper, "Evaluation of hair follicle parameters using TrichoScale Pro© in healthy dogs: a pilot study," Vet Dermatol **31**(3), 181–e137 (2020).
16. N. Kudlova, H. Slavik, P. Duskova, T. Furst, J. Srovnal, J. Bartek, M. Mistrik, and M. Hajduch, "An efficient, non-invasive approach for in-vivo sampling of hair follicles: design and applications in monitoring DNA damage and aging," Aging **13**, 25004–25024 (2021).
17. J. E. Plowman, "Diversity of trichocyte keratins and keratin associated proteins," Adv. Exp. Med. Biol. **1054**, 21–32 (2018).
18. R. A. Baus, C. Leichner, C. Steinbring, and A. Bernkop-Schnurch, "Strategies for improved hair binding: Keratin fractions and the impact of cationic substructures," Int. J. Biol. Macromol. **160**, 201–211 (2020).
19. N. Kariya, Y. Shimomura, and M. Ito, "Size polymorphisms in the human ultrahigh sulfur hair keratin-associated protein 4, KAP4, gene family," J. Invest. Dermatol. **124**(6), 1111–1118 (2005).
20. A. Pena, M. Strupler, T. Boulesteix, and M. Schanne-Klein, "Spectroscopic analysis of keratin endogenous signal for skin multiphoton microscopy," Opt. Express **13**(16), 6268–6274 (2005).
21. A. Ehlers, I. Riemann, M. Stark, and K. Konig, "Multiphoton fluorescence lifetime imaging of human hair," Microsc. Res. Tech. **70**(2), 154–161 (2007).
22. L. H. Laiho, S. Pelet, T. M. Hancewicz, P. D. Kaplan, and P. T. So, "Two-photon 3-D mapping of ex vivo human skin endogenous fluorescence species based on fluorescence emission spectra," J. Biomed. Opt. **10**(2), 024016 (2005).
23. K. Teuchner, W. Freyer, D. Leupold, A. Volkmer, D. J. Birch, P. Altmeyer, M. Stucker, and K. Hoffmann, "Femtosecond two-photon excited fluorescence of melanin," Photochem. Photobiol. **70**, 146–151 (1999).
24. S. M. Sternisha, P. Mukherjee, A. Alex, E. J. Chaney, R. Barkalifa, B. Wan, J. H. Lee, J. Rico-Jimenez, M. Zurauskas, D. R. Spillman Jr., S. A. Sripada, M. Marjanovic, Z. Arp, S. S. Galosy, D. S. Bhanushali, S. R. Hood, S. Bose, and S. A. Boppart, "Longitudinal monitoring of cell metabolism in biopharmaceutical production using label-free fluorescence lifetime imaging microscopy," Biotechnol. J. **16**, e2000629 (2021).
25. R. Penjweini, B. Roarke, G. Alspaugh, A. Gevorgyan, A. Andreoni, A. Pasut, D. L. Sackett, and J. R. Knutson, "Single cell-based fluorescence lifetime imaging of intracellular oxygenation and metabolism," Redox Biol. **34**, 101549 (2020).
26. J. D. Jones, H. E. Ramser, A. E. Woessner, A. Veves, and K. P. Quinn, "Quantifying age-related changes in skin wound metabolism using in vivo multiphoton microscopy," Adv. Wound Care **9**(3), 90–102 (2020).
27. H. Li, M. Yan, J. Yu, Q. Xu, X. Xia, J. Liao, and W. Zheng, "In vivo identification of arteries and veins using two-photon excitation elastin autofluorescence," J. Anat. **236**(1), 171–179 (2020).
28. Y. Sun, L. Li, S. Ma, G. He, W. Yang, and Y. Wang, "In vivo visualization of collagen transdermal absorption by second-harmonic generation and two-photon excited fluorescence microscopy," Front. Chem. **10**, 925931 (2022).
29. M. Seeger, C. Dehner, D. Justel, and V. Ntziachristos, "Label-free concurrent 5-modal microscopy (Co5M) resolves unknown spatio-temporal processes in wound healing," Commun. Biol. **4**(1), 1040 (2021).

Biomedical Optics EXPRESS

30. H. Zuhayri, V. V. Nikolaev, A. I. Knyazkova, T. B. Lepekhina, N. A. Krivova, V. V. Tuchin, and Y. V. Kistenev, "In vivo quantification of the effectiveness of topical low-dose photodynamic therapy in wound healing using two-photon microscopy," Pharmaceutics **14**(2), 287 (2022).
31. B. Sarri, X. Chen, R. Canonge, S. Gregoire, F. Formanek, J. B. Galey, A. Potter, T. Bornschlogl, and H. Rigneault, "In vivo quantitative molecular absorption of glycerol in human skin using coherent anti-Stokes Raman scattering (CARS) and two-photon auto-fluorescence," J. Controlled Release **308**, 190–196 (2019).
32. J. Ahn, K. H. Kim, K. Choe, J. H. Lim, S. K. Lee, Y. S. Kim, and P. Kim, "Quantitative two-photon microscopy imaging analysis of human skin to evaluate enhanced transdermal delivery by hybrid-type multi-lamellar nanostructure: retraction," Biomed. Opt. Express **11**(10), 5871 (2020).
33. L. Szyc, C. Scharlach, H. Haenssle, and C. Fink, "In vivo two-photon-excited cellular fluorescence of melanin, NAD(P)H, and keratin enables an accurate differential diagnosis of seborrheic keratosis and pigmented cutaneous melanoma," J. Biomed. Opt. **26**(07), 1 (2021).
34. V. D. Ching-Roa, C. Z. Huang, S. F. Ibrahim, B. R. Smoller, and M. G. Giacomelli, "Real-time analysis of skin biopsy specimens with 2-photon fluorescence microscopy," JAMA Dermatol. **158**(10), 1175–1182 (2022).
35. P. Rompolas, E. R. Deschene, G. Zito, D. G. Gonzalez, I. Saotome, A. M. Haberman, and V. Greco, "Live imaging of stem cell and progeny behaviour in physiological hair-follicle regeneration," Nature **487**(7408), 496–499 (2012).
36. C. M. Pineda, S. Park, K. R. Mesa, M. Wolfel, D. G. Gonzalez, A. M. Haberman, P. Rompolas, and V. Greco, "Intravital imaging of hair follicle regeneration in the mouse," Nat. Protoc. **10**(7), 1116–1130 (2015).
37. Y. Chen, Z. M. Fan, X. X. Wang, M. H. Mo, S. B. Zeng, R. H. Xu, X. S. Wang, and Y. J. Wu, "PI3K/Akt signaling pathway is essential for de novo hair follicle regeneration," Stem Cell Res. Ther. **11**(1), 144 (2020).
38. N. Sagawa, Y. Oshima, T. Hiratsuka, Y. Kono, T. Etoh, and M. Inomata, "Role of increased vascular permeability in chemotherapy-induced alopecia: In vivo imaging of the hair follicular microenvironment in mice," Cancer Sci. **111**(6), 2146–2155 (2020).
39. D. Fu, J. Huang, K. Li, Y. Chen, Y. He, Y. Sun, Y. Guo, L. Du, Q. Qu, Y. Miao, and Z. Hu, "Dihydrotestosterone-induced hair regrowth inhibition by activating androgen receptor in C57BL6 mice simulates androgenetic alopecia," Biomed. Pharmacother. **137**, 111247 (2021).
40. H. S. Shin, S. Y. Park, H. G. Song, E. Hwang, D. G. Lee, and T. H. Yi, "The androgenic alopecia protective effects of forsythiaside-a and the molecular regulation in a mouse model," Phytother. Res. **29**(6), 870–876 (2015).
41. L. Subedi, P. Pandey, J. H. Shim, K. T. Kim, S. S. Cho, K. T. Koo, B. J. Kim, and J. W. Park, "Preparation of topical bimatoprost with enhanced skin infiltration and in vivo hair regrowth efficacy in androgenic alopecia," Drug Delivery **29**(1), 328–341 (2022).
42. R. M. Trueb, "Molecular mechanisms of androgenetic alopecia," Exp. Gerontol. **37**(8-9), 981–990 (2002).
43. A. Rossi, A. Anzalone, M. C. Fortuna, G. Caro, V. Garelli, G. Pranteda, and M. Carlesimo, "Multi-therapies in androgenetic alopecia: review and clinical experiences," Dermatol. Ther. **29**(6), 424–432 (2016).
44. R. Sennett and M. Rendl, "Mesenchymal-epithelial interactions during hair follicle morphogenesis and cycling," Semin. Cell Dev. Biol. **23**(8), 917–927 (2012).
45. Q. Liu, Y. Tang, Y. Huang, J. Wang, K. Yang, Y. Zhang, W. Pu, J. Liu, X. Shi, Y. Ma, C. Ni, Y. Zhang, Y. Zhu, H. Li, J. Wang, J. Lin, and W. Wu, "Insights into male androgenetic alopecia using comparative transcriptome profiling: hypoxia-inducible factor-1 and Wnt/beta-catenin signalling pathways," Br. J. Dermatol. **187**(6), 936–947 (2022).
46. A. Premanand and B. Reena Rajkumari, "Androgen modulation of Wnt/beta-catenin signaling in androgenetic alopecia," Arch. Dermatol. Res. **310**(5), 391–399 (2018).
47. V. L. Truong, M. J. Bak, C. Lee, M. Jun, and W. S. Jeong, "Hair regenerative mechanisms of red ginseng oil and its major components in the testosterone-induced delay of anagen entry in C57BL/6 mice," Molecules **22**(9), 1505 (2017).
48. X. M. Hu, Z. X. Li, D. Y. Zhang, Y. C. Yang, S. A. Fu, Z. Q. Zhang, R. H. Yang, and K. Xiong, "A systematic summary of survival and death signalling during the life of hair follicle stem cells," Stem Cell Res. Ther. **12**(1), 453 (2021).
49. K. S. Stenn and R. Paus, "Controls of hair follicle cycling," Physiol. Rev. **81**(1), 449–494 (2001).
50. J. K. Oh, O. S. Kwona, M. H. Kim, S. J. Jo, J. H. Han, K. H. Kim, H. C. Eun, and J. H. Chung, "Connective tissue sheath of hair follicle is a major source of dermal type I procollagen in human scalp," J. Dermatol. Sci. **68**(3), 194–197 (2012).
51. H. Morinaga, Y. Mohri, M. Grachtchouk, K. Asakawa, H. Matsumura, M. Oshima, N. Takayama, T. Kato, Y. Nishimori, Y. Sorimachi, K. Takubo, T. Suganami, A. Iwama, Y. Iwakura, A. A. Dlugosz, and E. K. Nishimura, "Obesity accelerates hair thinning by stem cell-centric converging mechanisms," Nature **595**(7866), 266–271 (2021).
52. A. G. Messenger and J. Rundegren, "Minoxidil: mechanisms of action on hair growth," Br. J. Dermatol. **150**(2), 186–194 (2004).
53. J. Li, X. Wu, Y. Fu, H. Nie, and Z. Tang, "Two-photon microscopy: application advantages and latest progress for in vivo imaging of neurons and blood vessels after ischemic stroke," Rev. Neurosci. **34**(5), 559–572 (2023).
54. C. L. Chen, W. Y. Huang, E. H. C. Wang, K. Y. Tai, and S. J. Lin, "Functional complexity of hair follicle stem cell niche and therapeutic targeting of niche dysfunction for hair regeneration," J. Biomed. Sci. **27**(1), 43 (2020).
55. Y. J. Lee, S. H. Park, H. R. Park, Y. Lee, H. Kang, and J. E. Kim, "Mesenchymal stem cells antagonize IFN-induced proinflammatory changes and growth inhibition effects via Wnt/beta-Catenin and JAK/STAT pathway in human outer root sheath cells and hair follicles," Int. J. Mol. Sci. **22**(9), 4581 (2021).
56. P. Mirmirani, H. Uno, and V. H. Price, "Abnormal inner root sheath of the hair follicle in the loose anagen hair syndrome: an ultrastructural study," J. Am. Acad. Dermatol. **64**(1), 129–134 (2011).